Review

Influence of the oxygen pressure on the physical properties of the pulsed-laser deposited Te doped SnO$_2$ thin films

E. Chan y Díaz [a,*], Juan M. Camacho [b], A. Duarte-Moller [a], R. Castro-Rodríguez [b], P. Bartolo-Pérez [b]

[a] Centro de Investigación en Materiales Avanzados, S.C. (CIMAV), Miguel de Cervantes Saavedra 120, Complejo industrial Chihuahua, Chihuahua 31109, México
[b] Applied Physics Department, CINVESTAV-IPN, Unidad Mérida, 97310 Mérida, Yucatán, México

A B S T R A C T

Tellurium doped tin oxide (Te:SnO$_2$) thin films were prepared by pulsed-laser deposition (PLD) on glass substrates at different oxygen pressures, and the effects of oxygen pressure on the physical properties of as-grown and post-annealed Te:SnO$_2$ films were investigated. The as-grown films deposited between 1.0 and 50 mTorr showed some evidence of diffraction peaks, with electrical resistivity of $\sim 8 \times 10^1$ Ω cm, but increasing the oxygen pressure up to 100 mTorr, three diffraction peaks (1 1 0), (1 0 1) and (2 1 1) were observed containing the SnO$_2$ tetragonal structure, at 100 mTorr the electrical resistivity decreased abruptly at minimum value of 4×10^{-2} Ω cm, and increased reaching values of $\sim 4 \times 10^{-1}$ Ω cm. The optical transmittance of the films increased with increasing oxygen pressure and high transmittance ($\sim 87\%$) in VIS region by the films prepared at 100 mTorr and higher. The band gap of as-grown films was ~ 3.5 eV corresponding at of the SnO$_2$. After of post-annealed at 500 °C at atmospheric pressure for 30 min all films showed crystallization, and notable electrical resistivity changes were observed. The carrier density increased monotonically in the range of oxygen pressure between 1.0 and 100 mTorr, reaching values of $\sim 2 \times 10^{18}$ cm^{-3}, then, it decreased abruptly in films grown at 125 mTorr. While the mobility of the free-carrier decreased in the range of oxygen pressure between 1.0 and 100 mTorr, reaching minimum values of ~ 5.8 cm^2 V^{-1} s^{-1}. The optical transmittance showed similar characteristic like the as-grown films. The figure of merit at 100 mTorr of as-grown films had value $\sim 1.2 \times 10^{-5}$ Ω^{-1}, and for post-annealed films at 100 mTorr the figure of merit was similar $\sim 1.7 \times 10^{-6}$ Ω^{-1}, indicating they were the better films.

Contents

1. Introduction

Transparent conducting oxides (TCOs) are widely used for a variety of applications, including transparent electrodes for flat panel displays and for photovoltaic cell, low emissivity windows, windows defrosters, transparent thin films transistor, light emitting diodes, and semiconductor lasers [1–7]. Undoped tin oxide (SnO$_2$), which is a wide band gap (E_g) n-type semiconductor (3.6 eV) [8], belongs to the important family of oxide materials that combine low electrical resistance with high optical transparency (>80%) in the visible range (VIS) of the electromagnetic spectrum. SnO$_2$ films have some practical advantages over transparent conducting oxides (TCOs) films that contain indium or cadmium, as they are less expensive and non-toxic.

There are many different techniques used for deposition SnO$_2$ films: spray pyrolysis [9], reactive electron beam evaporation [10], rf-sputtering [11,12], dc-magnetron sputtering [13], chemical vapor deposition [14], reactive ion assisted deposition [15], filtered vacuum arc deposition [16] and pulsed-laser deposition (PLD) [17]. However, all methods require high substrate temperature or post-annealed in order to fabricate good-quality polycrystalline films. PLD has emerged as one of the simplest and most versatile meth-

* Corresponding author. Tel.: +52 614 439 1127; fax: +52 614 439 4884.
E-mail address: enrique.chan@cimav.edu.mx (E. Chan y Díaz).

ods for the deposition thin films of a wide variety of materials [18]. A major advantage of PLD is that the stoichiometry of the target can be retained in the deposited films. In particular PLD in oxidizing gases is one of the promising methods of preparing complex oxide films, and has been applied to the deposition of TCOs films as various high-quality SnO_2 thin films with low resistivity [19–21]. In all the techniques used for the fabrication of SnO_2 films, the structural, optical and electrical properties of the films have been found to depend critically on the oxygen partial pressures (PO_2) and the substrate temperature (T_s) [22,23].

As we know, TCOs have conductivity (σ) in the range 10^2–10^6 S cm^{-1}. The conductivity is due to doping either by oxygen vacancies (V_O) or by extrinsic dopant. In the absence of doping, these oxides become very good insulators, with resistivity (ρ) $> 10^{10}$ Ω cm. The electrical conductivity of n-type TCOs thin film depends on the carrier density in the conduction band and on their mobility: $\sigma = \mu n e$, where μ the electron mobility, n is the carrier density and e is the electron charge. Due to $E_g > 3.0$ eV separating the valence band from the conducting band, the conduction band cannot be thermally populated at room temperature ($kT \sim 0.03$ eV, where k is Boltzmann's constant), hence, stoichiometric crystalline TCOs are good insulators [7]. In the case of intrinsic materials, the density of conducting electrons has often been attributed to the presence of unintentionally introduced donor centers, usually identified as metallic interstitials (M_i) or oxygen vacancies (V_O) that produce shallow donor or impurity states located close to the conduction band. The excess of donor electrons is thermally ionized at room temperature, and move into the host conduction band. However, experiments have been inconclusive as to which of the possible dopants is the predominant donor [24]. Extrinsic dopant has an important role in populating the conduction band, and some of them have been unintentionally introduced.

On the other hand, a great variety of dopants have been studied in order to improve the electrical properties of SnO_2 for certain applications. The common extrinsic n-type dopants [11,12] are Sb, F, As, Nb and Ta. However, the electrical conductivity control of this material is not developed yet because there are problems that normally grown SnO_2 films seriously suffer from donor-type defects such a tin interstitial (Sn_i), V_O and these dopants impurities, which could deteriorates the mobility of the electron as consequence of a structural distortion due at the excess from a critical value of these donor-type defects. Tellurium is a semi metallic element with valence states of -2, $+4$ and $+6$ and is often used alloyed to Sn as SnTe, the multiple valences of the tellurium and its affinity with Sn can be used to tellurium doped SnO_2 as donor-type defect such a tellurium interstitial into SnO_2 structure and as consequence improve the electrical properties of the SnO_2.

Recently, it has been reported that the post-annealed process is also effective to reduce the residual donor-type defects on grown SnO_2 films in addition to the growth parameters such as surface treatment, substrate temperature, and Sn/O ratio [16]. In dependence of the technique of growth, usually the electron concentration varies with the annealing temperature and reaches minimum or maximum values in dependence of its temperature. This suggest that the increase and decrease of electron concentration is caused by to generation and reduction of V_O, also it suspected that this behavior is due to the reduction of Sn_i as has been observed in SnO_2 films grown by pulsed-laser deposition that electron concentration continuously decreases with the increase of annealing temperature [8,25]. These reports commonly refer that the annealing process under certain conditions is helpful for improve the structural properties of the films.

In this paper, we report on the investigation of the heat treatment on the physical properties of the Te-doped SnO_2 thin films grown by pulsed-laser deposition and the behavior of structural, electrical and optical properties.

2. Experimental procedure

Te-doped SnO_2 thin films were deposited on 25 mm $\times$ 25 mm glass substrates (Corning 2947) using a Nd:YAG laser (1064 nm, 10 ns full width at half-maximum) at a repetition rate of 5 Hz on a target with rotation of 30 rpm in order to avoid pitting of target at any given spot and to obtain uniform thin films. The substrate is attached with a stainless steel mask to the substrate holder which was heated by a tungsten lamp. The laser was focused through a 50 cm focal length lens onto a rotating target at a 45° angle of incidence. The energy density of the laser beam on the target surface was maintained at $\sim$2.0 J/cm^2. The target-to-substrate distance was 60 mm. Before laser irradiation the deposition chamber is evacuated down to a base pressure of 10^{-6} Torr using a diffusion pump and a rotary pump. The target was prepared from 1.0 wt.% Te powder (6 N) mixture with SnO_2 powder (5 N) and sintered (thickness of 0.5 mm and diameter of 15 mm). During deposition, high purity oxygen (99.997%) was introduced into the chamber at different pressures (ranging from 1.0 to 150 mTorr). Substrate temperature for all growths was maintained at 500 °C. The ablations shots for all films were 10^3. The substrates were carefully cleaned in an ultrasonic bath for 10 min with acetone and methanol, rinsed in deionized water, and subsequently dried in air before deposition.

After deposition, the substrate was maintained at 500 °C for 30 min with same PO_2 was grown and was cooled to room temperature in the base pressure. The film was divided into two equal parts, one was annealed at 500 °C for 30 min at atmospheric pressure in a muffle in order to compare their physical properties as-grown and after of post-annealed.

The thickness (d) of the films was measured by a surface profilometer Dektak-8, Veeco. The electrical properties were determined at room temperature by Van der Pauw-Hall method. For a uniform thickness, the electrical resistivity (()) can be determined using the relation ($ = R_{Sheet}d$, where R_{Sheet} is the sheet resistance. All sheet resistance and resistivity values were determined as the average of three measurements of three different films deposited at same conditions. The optical transmittance measurements were performed using VIS-near-IR spectrophotometer. The value of the direct band gap was calculated using transmittance measurements and the Tauc formalism for direct transitions and parabolic bands [26].

$$\left\{ h\nu \ln\left[\frac{T}{T'}\right]\right\}^2 = (Ad)^2 \, (h\nu - Eg) \tag{1}$$

where T is the film transmittance, T' is the substrate transmittance, A is a constant that depends on the material, d is the film thickness, $h\nu$ the photon energy and Eg the band-gap energy. In $\{h\nu \ln[T/T']\}^2$, $h\nu$ coordinates expression (1) is a straight line. The line intercept corresponds to the band-gap energy. The structural properties were determined by measurements in the grazing incidence geometry with an inclination of 1° in the X-ray diffraction beam (XRD) using CuKα wavelength monochromatic radiation ($\lambda = 1.5405$ Å), at 40 kV with 35 mA and with an aperture diaphragm of 0.2 mm, using a D5000 Siemens X-ray diffractometer. XPS analyses were performed in a Perkin-Elmer PHI 560/ESCA-SAM system, with a base pressure of 2×10^{-9} Torr. Argon ion sputtering was performed with 4 keV energy ions and 0.36 μA/cm^2 current beam, yielding to about 3 nm/min sputtering rate. All XPS spectra were obtained without erosion and after 10 min of Ar$^+$ sputtering. The spectrometer was calibrated using the Cu 2p$_{3/2}$ (932.4 eV) and Cu 3p$_{3/2}$ (74.9 eV) lines. Binding energy calibration was based on C 1s at 284.6 eV.

3. Results and discussion

Fig. 1 shows the XRD patterns of as-grown films at 500 °C in different PO_2. The films deposited between 1.0 and 50 mTorr show evidence of three diffraction peaks around 2θ at 26.6° (1 1 0), 33.8° (1 0 1) and 51.7° (2 1 1), but when increasing the PO_2 up to 100 mTorr these orientations becomes more evident. All the films up to 100 mTorr are polycrystalline and contain the SnO_2 tetragonal structure [27]. It is observed the effect of PO_2 on the crystallinity of the Te:SnO_2 films, the intensity of (1 1 0) and (1 0 1) diffraction peak increases with increasing PO_2, but the (1 1 0) diffraction peak decreases for $PO_2 = 125$ mTorr, increasing the (1 0 1) diffraction peak. A strong peak signal of the (1 1 0) was observed for the 100 mTorr film, while the less intense was for the film prepared at 125 mTorr.

Fig. 2 shows the XRD patterns as a function of PO_2, of the post-annealed films. As it can be observed in the figure, all films have better crystallization than those without treatment, so the heat treatment improves the crystalline properties. At particular, the grown film at 10 mTorr has high orientation in the plane (1 1 0), but at higher pressures than 50 mTorr the peaks (1 1 0) decrease and the plane (1 0 1) increases evidently, indicating the crystal reori-
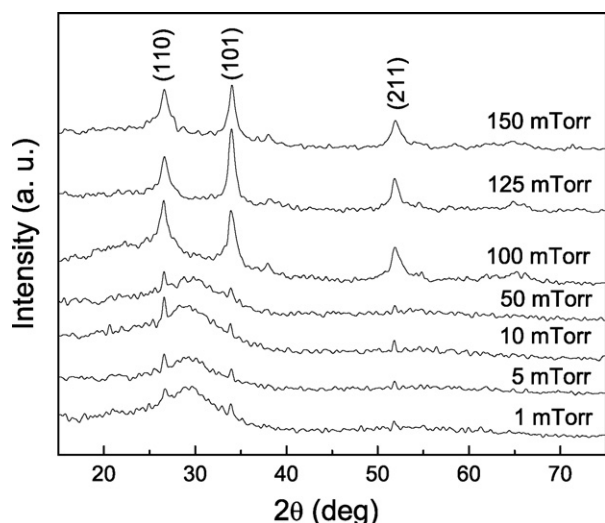
Fig. 1. XRD patterns of as-grown Te:SnO$_2$ films.

entation effect. This means that the heat treatment reduces the isolated point defects and the conglomerated extended defects, which improve the crystallinity of the films.

Additional information is given from the XRD measurements by calculating the crystal size of SnO$_2$ film using Scherreřs formula [28]

$$D = \frac{0.9\lambda}{\beta \cos\theta} \qquad (2)$$

where λ is the X-ray wavelength (1.5402 Å), β is the (1 1 0) peak width (in radians), D is the crystal size, and θ is the Bragg diffraction angle. Table 1 shows that the crystal size increases from 18.08 nm at 1 mTorr to 24.19 nm at 50 mTorr, and then decreases gradually for films prepared up to 50 mTorr. This suggests that the crystalline quality of the films is degraded with the increase in PO_2. The excess oxygen might induced defects in the films, which have influence on the nucleation and the growth of the films and as resulted in the degradation of the crystalline quality. These results also confirm that a pressure of 50 mTorr it will give better epitaxy, better texture and a larger crystal size of 24.19 nm in the films. On the other hand, the crystal sizes have similar values (see Table 1) for the treated films. The as-grown and post-annealed films shown minor volume
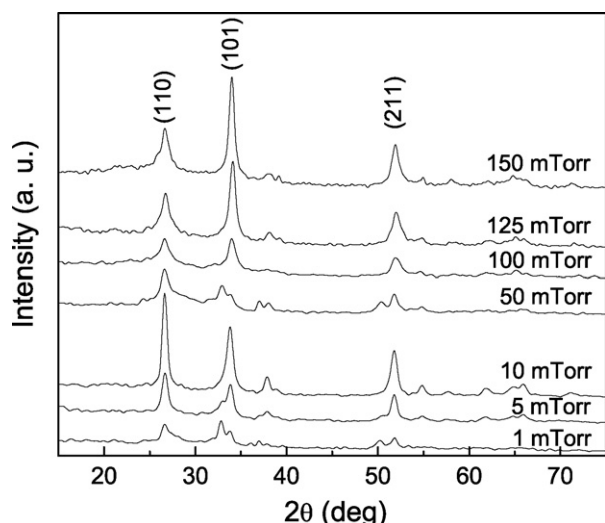

Fig. 2. XRD patterns of post-annealed Te:SnO$_2$ films.
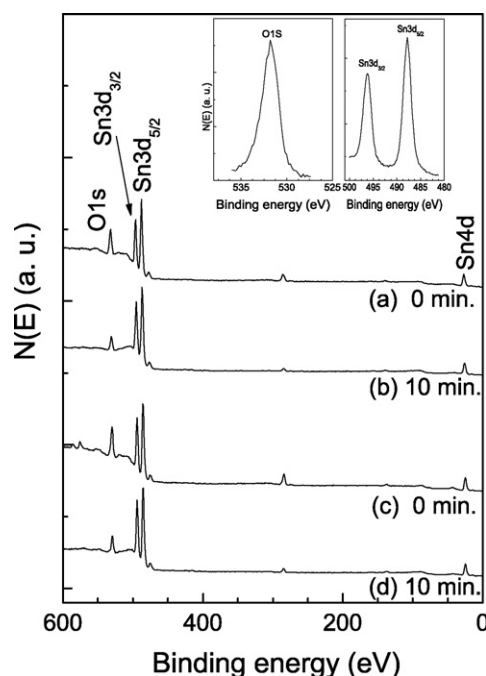

Fig. 3. XPS spectra of the typical Te:SnO$_2$ thin films deposited at 50 mTorr, (a) and (b) as-grown, (c) and (d) post-annealed. The insets show the O 1S and Sn3d in high resolution.

of the unit cell than the SnO$_2$ powder (71.55 Å^3), by indicating a compression of the unit cell due at the V_O formation. It is clear that the volume of the unit cell is not significantly affected by Te-doped. Since the ionic radius of Te^{+4} and Te^{+6} ($\sim$2.21 Å) is more large that of Sn^{+4} (0.71 Å), so the Te atoms can not to be incorporate in Sn vacancies, but can incorporate in interstitial sites and produce a tensile stress. We conclude that the incorporation of Te atoms into the SnO$_2$ structure is very poor, this is due to that only 1.0 wt.% of Te was mixture in the SnO$_2$ target.

In order to confirm oxidation on the surface and bulk of the films, XPS analysis was performed. In Fig. 3, XPS survey spectra of films grown at 50 mTorr without (0 min) and after 10 min of Ar$^+$ sputtering are presented. Fig. 3(a) and (b) corresponds at the as-grown films, (c and d) corresponds at the post-annealed films. In this figure, the O 1 s (531 eV), Sn 3d$_{3/2}$ (495 eV) and Sn 3d$_{5/2}$ (487 eV) core level principal peaks can be observed. Also, the Sn 4d (26 eV) secondary peak is detected. As can observed, the peak O 1s corresponding at the surface of the films is more intense that the signal of the peaks after 10 min of erosion, indicating that there are more oxidation in the surface that in the bulk of the films. Similar results can be observed in the other samples.

Relative atomic surface concentrations were determined using the integrated area under O 1s and Sn 4d$_{5/2}$ and the common formula for the relative atomic concentrations [29]. Results of the calculations of relative atomic concentration are presented in Table 2. The effect of reorientation from plane (1 1 0) to plane (1 0 1) observed in Fig. 2 can be explained by the variation oxygen concentration as can observed in Table 2. Significant oxygen variations induce significant V_O variations that can induce a structural stress, causing a reorientation planes of the crystalline lattice. The binding energy of Sn 3d$_{5/2}$ peak was E_B = 487 eV that corresponds to a fully oxidized Sn^{+4} state [30]. Also, the binding energy of O 1 s peak was E_B = 531 eV that corresponds to O^{-2} state (see inset in Fig. 3). Therefore the SnO$_2$ compound is formed.

Thickness variation of the films is shown in Fig. 4. The rate deposition is affected by the scattering of the ablated species, the as-grown films show a thickness variation between 41 and 258 nm.

Table 1
Structural properties of Te:SnO$_2$ films on glass substrates at 500 °C as a function of PO_2.

As-grown					Post-annealed			
PO_2 (mTorr)	Crystal size (nm)	$a = b$ (Å)	c (Å)	V (Å^3)	Crystal size (nm)	$a = b$ (Å)	c (Å)	V (Å^3)
SnO$_2$	–	4.7382	3.1871	71.55	–	4.7382	3.1871	71.55
1	18.08	4.7115	3.1900	70.81	15.75	4.7248	3.2047	71.54
5	20.51	4.7305	3.1779	71.12	11.95	4.7214	3.1969	71.26
10	20.74	4.7315	3.1915	71.45	13.13	4.7270	3.2018	71.54
50	24.19	4.7333	3.1834	71.32	11.20	4.7246	3.2025	71.49
100	11.62	4.7479	3.1670	71.39	12.16	4.7283	3.1718	70.91
125	10.76	4.7262	3.1731	70.88	8.93	4.7141	3.1655	70.34
150	11.23	4.7285	3.1677	70.82	11.78	4.7207	3.1762	70.78
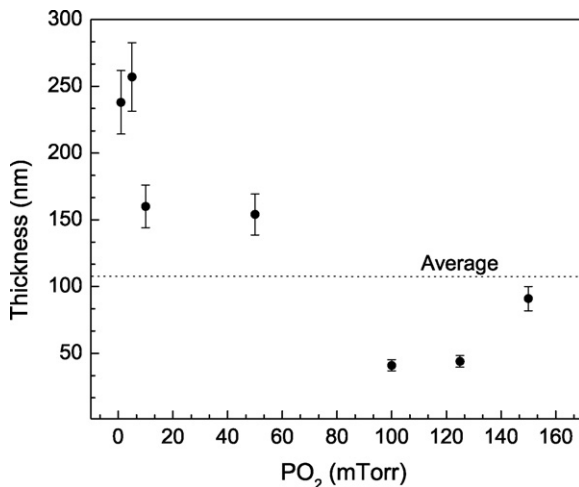
Fig. 4. Thickness for the Te:SnO$_2$ films as a function of the oxygen pressure.

The thickness of the films reduces significantly when increase the PO_2. The reduction in the rate deposition is attributed primarily to collisions of the ablated tin, tellurium and oxygen particles with the ionized gas plasma during deposition [31].

The electrical resistivity of the as-grown and post-annealed films is shown in Fig. 5. For as-grown films deposited between 1.0 and 50 mTorr, the resistivity was $\sim 8 \times 10^1$ Ω-cm. Increasing PO_2 at 100 mTorr the resistivity decreases abruptly at minimum value of 4×10^{-2} Ω cm, and increasing again PO_2 the value of the resistivity increases reaching values of $\sim 4 \times 10^{-1}$ Ω cm. For post-annealed films deposited between 1.0 and 10 mTorr the resistivity
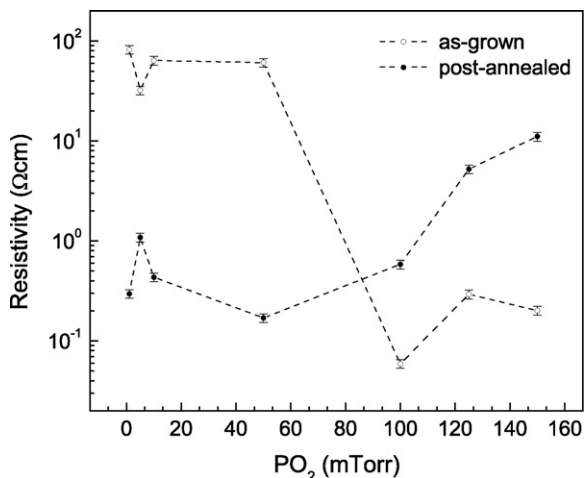
Fig. 5. Electrical resistivity as a function of PO_2 for as-grown and post-annealed Te:SnO$_2$ films, respectively.

was $\sim 6 \times 10^{-1}$ Ω cm and for PO_2 at 50 mTorr, the resistivity was $\sim 10^{-1}$ Ω cm. A significant diminution in resistivity is observed between as-grown and post-annealed films in the range of 1.0 and 50 mTorr. However, the resistivity of post-annealed films grown at PO_2 between 100 and 150 mTorr, increased. The change in the resistivity induced by the post-annealed treatment is related to the annihilation and formation of intrinsic donor-type defects, disproportion of residual impurities in the films or by the incorporation of extrinsic impurities as Te. These defects are dominant between 1.0 and 50 mTorr. However, these effects are contrary between 100 and 150 mTorr where the resistivity increase in the post-annealed films in comparison with the as-grown films. In SnO$_2$, the important role of Sn$_i$ in populating the conduction band, in addition to the V_O has been conclusively supported by first-principle calculation of Kiliç and Zunger [32]. They showed that Sn$_i$ and V_O, which dominated the defect structure of SnO$_2$ due to the multi-valence of Sn, explained the natural non-stoichiometry of this material and produce shallow donor levels, turning the material into an intrinsic n-type semiconductor. For films post-annealed in the range of 1.0 and 50 mTorr, we think that the Sn$_i$ and V_O increased but in the region of 100 and 150 mTorr, these defects decreased. This suggested that the behavior of resistivity is ascribed to the generation and reduction of Sn$_i$ and V_O. This observation is supported by the crystallization of the films in the region of 1.0 and 50 mTorr as shown in Fig. 2, by confirming that the treatment is effective to increase donor-type defects of the films grown by PLD at low PO_2. In the films, we think that the resistivity is not affected by the tellurium dopants due to the poor 1.0 wt.% tellurium-mixture in the SnO$_2$ target. On the other hand, Dolbec et al. [33] found that the electrical conduction of the PLD SnO$_2$ films is most likely influenced by free-carrier scattering at grain boundaries. The slight ρ variations observed by Dolbec over the substrate temperature range between 300 and 600 °C can be related to their corresponding film microstructures. Moreover, not only the grain size but also the film nanoporosity is highly influenced by the presence of a background gas pressure during the deposition of SnO$_2$ films.

Fig. 6 shows the carrier density and Hall mobility for post-annealed films as function of PO_2. The carrier density increases monotonically in the range PO_2 between 1.0 and 100 mTorr, exception of the film grown at 5.0 mTorr, reaching values of $\sim 2 \times 10^{18}$ cm^{-3}, up to 125 mTorr, the carrier density decreases abruptly. While the mobility of the free-carrier decreases in the range of PO_2 between 1.0 and 100 mTorr, exception of the grown film at 5.0 mTorr, reaching minimum values of ~ 5.8 cm^2 V^{-1} s^{-1}.

Table 2
Atomic concentrations of Te:SnO$_2$ thin films.

Erosion time (min)	As-grown		Post-annealed	
	O (%)	Sn (%)	O (%)	Sn (%)
0	71.8	28.2	76.2	23.8
10	54.6	45.4	60.4	39.6
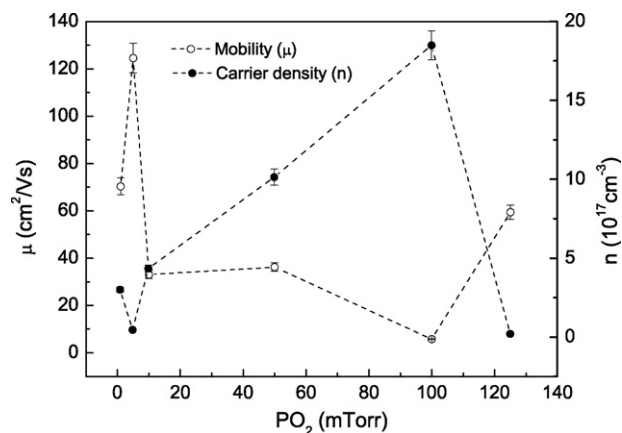
Fig. 6. Carrier density (n) and Hall mobility (μ) as a function of PO_2 for treated films.

Fig. 8. Optical transmittance spectra of treated films at different PO_2.

After, the mobility increases for grown films at 125 mTorr. The conductivity is intrinsically limited for two reasons: first, n and μ cannot be independently increased for TCOs with relatively high carrier concentration. At high conducting electron density, carrier transport is limited primarily by ionized impurity scattering. Higher doping concentration reduces carrier mobility to a degree that the conductivity is not increase. These observations are shown in combination of Figs. 5 and 6.

The optical transmittance in the VIS region of spectrum solar of the as-grown films is shown in Fig. 7. The optical transmittance of the films increases with increasing PO_2 and high transmittance (~87%) in VIS region was exhibited by the films prepared under PO_2 of 100 mTorr and higher. The optical band gaps of these films were ~3.5 eV corresponding at band gap of the SnO_2. At lower PO_2 resulted in translucent films with yellow color (~2.8 eV). Fig. 8 shows the optical transmittance of the treated films under different PO_2, as we can see at lower PO_2 (from 1.0 to 50 mTorr) there is strong shift of optical band gap to lower wavelengths. The optical band gap of the as-grown and post-annealed films is shown in Fig. 9. The band gap showed similar values for the prepared films at PO_2 of 100 mTorr and higher.

A figure of merit for a TCO may be defined by the ratio of the electrical conductivity to the optical absorption coefficient of the film. Common to all TCOs applications figure of merit is the need for optimizing the electrical and optical coating parameters. Depending on the type of device requiring a transparent electrode, the
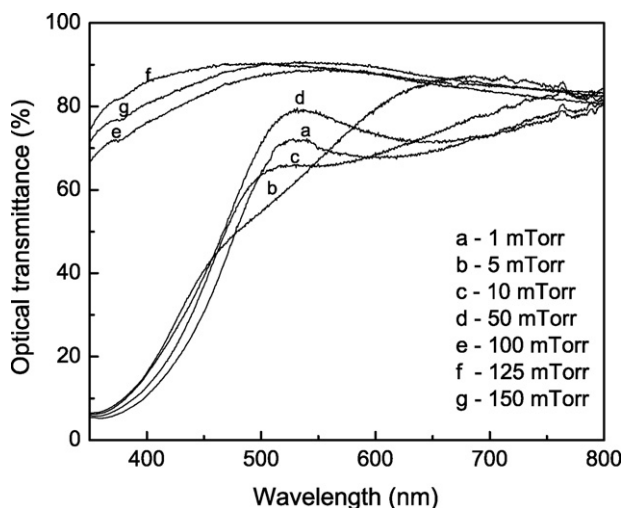

Fig. 9. Optical band gap as a function of PO_2 for as-grown and post-annealed films.

Fig. 7. Optical transmittance spectra of as-grown films at different PO_2.
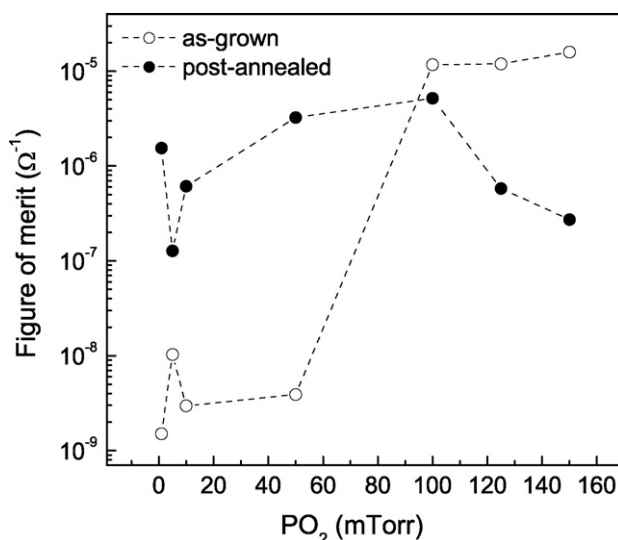

Fig. 10. Figure of merit as a function of PO_2 for as-grown and post-annealed films.

optical transmission and the electrical conduction of the electrodes should exceed certain minimum values. Ideally both parameters should be as large as possible but their inter-relationship usually excludes the simultaneous achievement of both these criteria [34]. In order to compare the performance of various TCOs it was used, the most widely used figure of merit of Haacke, defined as T^{10}/R_{sheet}, where the optical transmission (T) is take average around of 500 nm (near the solar spectrum maximum) [35,36]. Fig. 10 shows the figure of merit of the as-grown and post-annealing films deposited in different PO_2. For as-grown films deposited between 1.0 and 50 mTorr, the figure of merit was $\sim 4.6 \times 10^{-9}\,\Omega^{-1}$. Increasing PO_2 up to 100 mTorr the figure of merit increasing at maximum value of $\sim 1.2 \times 10^{-5}\,\Omega^{-1}$. For all post-annealed films deposited the figure of merit was $\sim 1.7 \times 10^{-6}\,\Omega^{-1}$. A notable increase is observed between as-grown and post-annealed films in the range of 1.0 and 50 mTorr. However, the figure of merit of post-annealed films grown with PO_2 between 100 and 150 mTorr, decreased. The best films were for as-grown and post-annealed films corresponding at 100 mTorr, with the major figure of merit.

4. Conclusion

Tellurium doped tin oxide thin films have been deposited by PLD on glass substrates. The physical properties of these films as-grown and with post-annealed treatment were investigated as a function of the oxygen pressure. The XRD results indicate that a post-annealed improves the crystallinity of the films. Especially, it should be noted that the preferential orientation of the films is changed from the (1 1 0) plane for low oxygen pressure to the (1 0 1) plane for higher pressure. The oxygen pressure between 50 and 100 mTorr reduce lattice structural disorders and hence increase the conductivity in as-grown films. However, oxygen pressure above that 100 mTorr result in less oxygen vacancies and decrease the conductivity of the films. After of post-annealed, a resistivity diminution is observed in the range of 1.0 and 50 mTorr, but the resistivities of films deposited between 100 and 150 mTorr, increased. The optical transmittance in visible region of films increased with an increase of oxygen pressure, and it was exhibited high values ($\sim 87\%$) by the as-grown and post-annealed films prepared under oxygen pressure of 100 mTorr and higher. A shift of absorption band near-UV is observed for all films after of post-annealed, consequently, the band gap of these films was ~ 3.5 eV corresponding at band gap of the SnO_2. In conclusion, we confirm that the annealing process is effective to increase donor-type defects of the films grown by PLD.

Acknowledgments

References

[1] K. Bädeker, Ann. Phys. (Leipzig) 22 (1907) 749–766.
[2] G. Haacke, Ann. Rev. Mater. Sci. 7 (1977) 73–93.
[3] M. Hiramatsu, K. Imaeda, N. Horio, M. Nawata, J. Vac. Sci. Technol. A 16 (1998) 669–673.
[4] B.G. Lewis, D.C. Paine, MRS Bull. (2000) 22–27.
[5] G.J. Exarhos, X.D. Zhou, Thin Solid Films 515 (2007) 7025–7052.
[6] E. Fortunato, D. Ginley, H. Hosono, D.C. Paine, MRS Bull. 32 (2007) 242–247.
[7] P.P. Edwards, A. Porch, M.O. Jones, D.V. Morgan, R.M. Perks, Dalton Trans. 19 (2004) 2995–3002.
[8] M. Batzill, U. Diebold, Prog. Surf. Sci. 79 (2005) 47–154.
[9] K.S. Shamala, L.C. Murthy, K. Narasimha Rao, Bull. Mater. Sci. 27 (3) (2004) 295–301.
[10] R. Banerjee, D. Das, Thin Solid Films 149 (1987) 291–301.
[11] B. Stjerna, E. Olsson, G. Granqvist, J. Appl. Phys. 76 (1994) 3797–3817.
[12] Sung Uk Lee, Byungyou Hong, Won Seok Choi, J. Vac. Sci. Technol. A 27 (2009) 996–1000.
[13] G.G. Mandayo, E. Castano, F.J. Gracia, A. Cirera, A. Cornet, J.R. Morante, Sens. Actuators B 95 (2003) 90–96.
[14] D. Davazoglou, Thin Solid Films 302 (1997) 204–213.
[15] W.K. Choi, H.-J. Jung, S.-K. Koh, J. Vac. Sci. Technol. A 14 (2) (1996) 359–366.
[16] E. Cetinörgü, S. Goldsmith, Y. Rosenberg, R.L. Boxman, J. Non-Cryst. Solids 353 (2007) 2595–2602.
[17] R.D. Vispute, V.P. Godbole, S.M. Chaudhari, S.M. Kanetkar, S.B. Ogale, J. Mater. Res. 3 (1988) 1180–1186.
[18] S.B. Ogale, Thin Films and Heterostructures for Oxide Electronics, First ed., Springer US, New York, 2005.
[19] C.K. Kim, S.M. Choi, I.H. Noh, J.H. Lee, C. Hong, H.B. Chae, G.E. Jang, H.D. Park, Sens. Actuators B 77 (2001) 463–467.
[20] Y. Suda, H. Kawasaki, J. Namba, K. Iwatsuji, K. Doi, K. Wada, Surf. Coat. Technol. 175 (2003) 1293–1296.
[21] R. Dolbec, M.A. El Khakani, A.M. Serventi, R.G. Saint-Jacques, Sens. Actuators B 93 (2003) 566–571.
[22] R. Khandelwal, A. Pratap Singh, A. Kapoor, S. Grigorescu, P. Miglietta, N.E. Stankova, A. Perrone, Opt. Laser Technol. 41 (2009) 89–93.
[23] Minju Ying, Yueyuan Xia, Yuming Sun, Mingwen Zhao, Xiangdong Liu, Opt. Lasers Eng. 41 (2004) 537–544.
[24] D.C. Look, B. Claflin, In: G.J. Brown, M.O. Manasreh, C. Gmachl, R.M. Biefeld, K. Unterrainer (Eds.), Progress in Compound Semiconductor Materials IV – Electronic and Optoelectronic Applications, Boston, USA, 2004, MRS Symposium Proceedings, vol. 829, 2005, p. B8.6.1.
[25] H. Kim, R.C.Y. Auyeung, A. Piqué, Thin Solid Films 516 (2008) 5052–5056.
[26] J. Tauc, R. Grigorovici, A. Vancu, Phys. Status Solid 15 (1966) 627–637.
[27] JCPDS – International Center Diffraction Data, 2005, PDF Card No. 41-1445.
[28] B.D. Cullity, S.R. Stock, Elements of X-ray Diffraction, Prentice Hall, 2001, p. 170.
[29] P. Bartolo-Pérez, J.L. Peña, M.H. Farias, Rev. Mex. Fis. 44 (1998) 9–23.
[30] P. Hanys, P. Janecek, V. Matolín, G. Korotcenkov, V. Nehasil, Surf. Sci. 600 (2006) 4233–4238.
[31] F.O. Adurodija, H. Izumi, T. Ishihara, H. Yoshioka, K. Yamada, H. Matsui, M. Motoyama, Thin Solid Films 350 (1999) 79–84.
[32] Ç. Kiliç, A. Zunger, Phys. Rev. Lett. 88 (2002) 095501.
[33] R. Dolbec, M.A. El Khakani, A.M. Serventi, M. Trudeau, R.G. Saint-Jacques, Thin Solid Films 419 (2002) 230–236.
[34] A.L. Dawar, J.C. Joshi, J. Mat. Sci. 19 (1984) 1–23.
[35] G. Haacke, J. Appl. Phys. 47 (1976) 4086–4089.
[36] S.S. Shinde, P.S. Shinde, C.H. Bhosale, K.Y. Rajpure, J. Phys. D: Appl. Phys. 41 (2008) 105109.